Dynamical downscaling of Typhoon Lionrock (2016) for assessing the resulting hazards under global warming

AUTHOR(S):

Nayak, Sridhara; Takemi, Tetsuya

Journal of the Meteorological Society of Japan, **97**(1), 69−88, 2019. doi:10.2151/jmsj.2019-003
Special Edition on Tropical Cyclones in 2015−2016

Dynamical Downscaling of Typhoon Lionrock (2016) for Assessing the Resulting Hazards under Global Warming

Sridhara NAYAK and Tetsuya TAKEMI

Disaster Prevention Research Institute, Kyoto University, Kyoto, Japan

(Manuscript received 1 April 2018, in final form 27 September 2018)

Abstract

Typhoons are considered as one of the most powerful disaster-spawning weather phenomena. Recent studies have revealed that typhoons will be stronger and more powerful in a future warmer climate and be a threat to lives and properties. In this study, we conduct downscaling experiments of an extreme rain-producing typhoon, Typhoon Lionrock (2016), to assess the impacts of climate change on resulting hazards by assuming pseudo global warming (PGW) conditions. The downscaled precipitations over the landfall region in the present climate condition agree well with the Radar-Automated Meteorological Data Acquisition System (Radar-AMeDAS) observations. A typhoon track in the future climate similar to that in the present climate is successfully reproduced, with a stronger wind speed (by ~ 20 knots) and lower central pressure (by ~ 20 hPa) under the PGW condition. The changes in precipitation amounts associated with the typhoon under PGW condition are analyzed over seven individual prefectures in the northern part of Japan. The typhoon in the warming climate produces more precipitation over all prefectures. Iwate, Aomori, Akita, Miyagi, and Hokkaido are projected to have relatively more precipitation associated with the typhoon in the warming climate. The overall analysis suggests that Typhoon Lionrock under PGW may increase the risk of flooding, damages to infrastructures, and lives staying along the typhoon track.

Keywords impact assessment; dynamical downscaling; pseudo global warming experiment; typhoon; typhoon hazard

Citation Nayak, S., and T. Takemi, 2019: Dynamical downscaling of Typhoon Lionrock (2016) for assessing the resulting hazards under global warming. *J. Meteor. Soc. Japan*, **97**, 69–88, doi:10.2151/jmsj.2019-003.

1. Introduction

Typhoons are considered one of the most powerful and devastating weather phenomena that cause severe and widespread damages such as loss of lives, economics, health, and habitats (e.g., Nishijima et al. 2012; Staid et al. 2014; Takemi et al. 2016c; Kure et al. 2016; Chen et al. 2018; Guan et al. 2018). The typhoons form over the western North Pacific Ocean and are directed by the Pacific subtropical high-pressure system. Over the years, a large number of typhoons originate over the western North Pacific region every year and a few of them were the most powerful, for example, Typhoon Vera (1959), Typhoon Mireille (1991), Typhoon Songda (2004), and Typhoon Haiyan (2013) and made landfall with strong winds and heavy precipitation (Oku et al. 2010; Mori et al. 2014; Takemi et al. 2016a, b; Kanada et al. 2017a). Such extreme typhoons strongly influence human lives, residential houses and urban buildings, agriculture, and industries at local scales (e.g., Nishijima et al. 2012; Staid et al. 2014). So, an increasing number of studies have conducted high-resolution downscaling simula-

Corresponding author: Sridhara Nayak, Disaster Prevention Research Institute, Kyoto University, Gokasho, Uji, Kyoto 611-0011, Japan
E-mail: nayak.sridhara.2n@kyoto-u.ac.jp
J-stage Advance Published Date: 29 October 2018

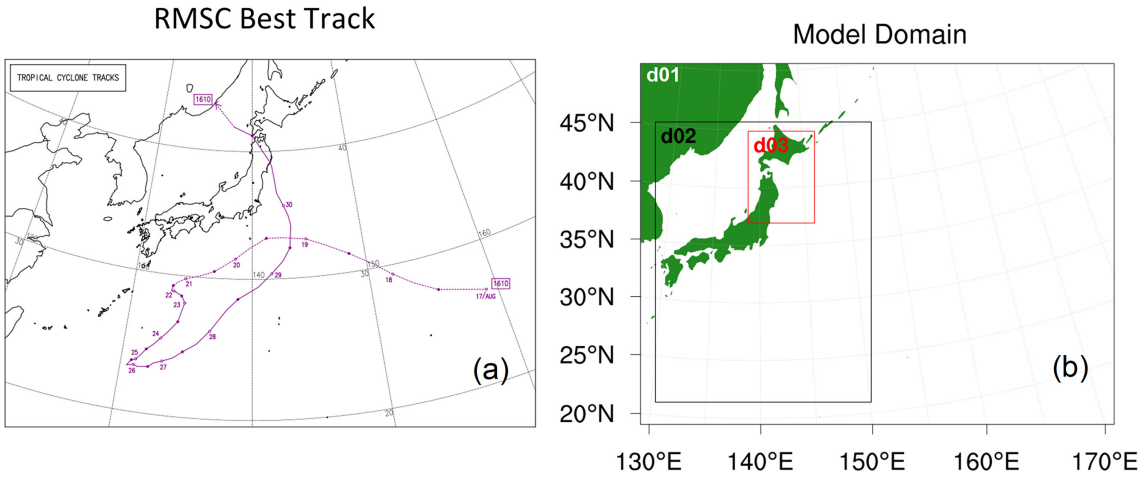

Fig. 1. (a) Typhoon track adopted from RSMC Tokyo best track figures; (b) model domain with three nests (d03 at 1 km; d02 at 3 km; and d01 at 9 km grid spacing).

tions (e.g., Lavender and Walsh 2011; Takemi et al. 2016a; Nakamura et al. 2016; Kanada et al. 2017b) to assess the impacts of the destructive typhoons on natural disasters not only in the present climate but also under future climate scenarios. In a recent study, Takemi et al. (2016a) conducted numerical simulations of Typhoon Mireille (1991) at 1 km spatial resolution in the present climate and under pseudo global warming (PGW) conditions. PGW conditions refer to the climate change components that are added to present analysis fields (Sato et al. 2007). Their results indicated that mean wind speeds induced by the typhoon are expected to be stronger in warmer climate conditions over Kyushu Island and weaker over the Tohoku region of Japan. In another study, Takemi et al. (2016b) investigated the influences of global warming on Typhoon Vera (1959) at 1-km grid resolution and highlighted that the intensity of the typhoon was stronger under PGW conditions. Multitudes of other studies such as Typhoon Songda (2004) (Ito et al. 2016), Typhoon Haiyan (2013) (Takayabu et al. 2015), and Typhoon Chanthu (2016) (Kanada et al. 2017a) also show stronger winds and/or heavy rainfall events in a warmer climate.

Recently, a typhoon, named as Lionrock (international number: 1610), had an unusual track and affected Japan, China, and Korean Peninsula during August 2016, with economic losses of about $325 million USD and at least 550 lives (Aon Benfield 2016). Based on the Regional Specialized Meteorological Center (RSMC), Tokyo's best track datasets, Typhoon Lionrock formed in the southeast of the northwestern Pacific region, originated at (27N, 157E) on 17 August, 2016, and moved westward until 20 August, then toward southwest until 26 August and intensified into a typhoon. Then, it moved toward the northeast and became a significant typhoon (See Fig. 1a) and made landfall at the east coast of Japan on 30 August. The maximum wind was observed as 90 knots on 28 August with a minimum central pressure of 940 hPa. This typhoon was the first typhoon that hit from Pacific Ocean side of the Tohoku region of Japan among the records (since 1951) available at Japan Meteorological Agency (JMA). Moreover, this typhoon approached from the southeast (the only typhoon after Typhoon Mac in 1989), while most of the typhoons that made landfall over Japan came either from the southwest or south and moved toward the north.

According to recent studies (e.g., Sugi et al. 2002; Emanuel 2005; Knutson et al. 2010; Mendelsohn et al. 2012; Murakami et al. 2012; IPCC 2013, 2014; Yamada et al. 2017), the frequency and intensity of typhoons are expected to increase under future warmer climate over the northwest Pacific Ocean. The studies indicate that the typhoons will be more intense in future climate and become a severer threat to lives and properties (e.g., Staid et al. 2014; Mei and Xie 2016). Therefore, to assess the impacts of threatening typhoons in future climate, high-resolution projection data with controlled typhoon track are necessary (e.g., Mori and Takemi 2016). Although simulating the typhoon tracks under future climate has been a challenging issue due to their varied nature of genesis location

and intensity, several studies, such as mentioned earlier (e.g., Oku et al. 2010; Takayabu et al. 2015; Takemi et al. 2016a, b; Kanada et al. 2017a), have conducted very high-resolution simulations of several devastating typhoons that made landfall over Japan mainly for the purpose of impact assessment over the typhoon-affected regions in present and future climate. However, few studies have been conducted to provide very-high-resolution downscaling experiments of typhoons that affected the higher-latitude regions, i.e., the northern part of Japan. Ito et al. (2016) and Kanada et al. (2017a) examined the impacts of global warming on extreme typhoons, i.e., Typhoon Songda (2004) and Typhoon Chanthu (2016), respectively, which spawned severe disasters in the northern part of Japan. It is very important to investigate various types of typhoons in order to reveal robust features of typhoon hazards under global warming. In this sense, Typhoon Lionrock (2016) should add new insights to the impact assessment of typhoon hazards, because the typhoon with a rare track and landfall location spawned extreme precipitation in the northern part of Japan.

Thus, we attempted to perform dynamical downscaling simulations of Typhoon Lionrock (2016) at 1 km grid resolution for a target region in the northern part of Japan by using the Weather Research and Forecasting (WRF) model. We will discuss: (1) the typhoon track and intensity of Typhoon Lionrock and the associated wind speed and precipitation amount in the target region after landfall; (2) the typhoon's response to the climate change under PGW conditions.

The next section describes the model setup and its configuration. The subsequent sections present the results and related discussions.

2. Model configuration

2.1 Model setup

The Advanced Research Weather Research and Forecasting (WRF) (WRF-ARW) version 3.8.1 (Skamarock et al. 2008) is configured with three nested domains (See Fig. 1b). The parent domain, having the horizontal resolution of 9 km, covers the Japanese islands and the westernmost part of the North Pacific Ocean; the inner middle domain with the resolution of 3 km covers whole Japan; and the innermost domain with the resolution of 1 km covers the target region of our study, i.e., the northern part of Japan. Two-way nesting was used for the interaction between the parent and the inner domain. To incorporate the synoptic-scale influences in the outer domain, we used spectral nudging technique with five wave number in the x and y directions. The physics parameterizations used in the model include the Kain-Fritsch cumulus scheme (Kain and Fritsch 1993), the WRF single moment 6-class (WSM6) microphysics scheme (Hong and Lim 2006), and the Yonsei University (YSU) planetary boundary scheme (Hong et al. 2006). All the domains are comprised of 28 vertical levels with the model top at 10 hPa. An overview of the model configuration is given in Table 1.

Table 1. Overview of the model setup and configuration used in this study.

Dynamics	Non-hydrostatics
Domain size	130–170E, 20–50N, 130–150E, 21–45N, 138–146E, 37–45N
Simulation period	00 UTC 26 August 2016 –00 UTC 31 August 2016
Grid resolution	9 km, 3 km, 1 km
Map projection	Lambert
Time step	30 seconds
Vertical level	28
Microphysics	WSM 6-class scheme (Hong and Lim 2006)
Cumulus scheme	Kain-Fritsch new Eta scheme (Kain and Fritsch 1993)
PBL scheme	YSU scheme (Hong et al. 2006)
Radiation scheme	Rapid Radiative Transfer Model (RRTM) scheme (Mlawer et al. 1997)

2.2 Data

Either the European Centre for Medium-Range Weather Forecasts (ECMWF) Reanalysis (ERA-Interim) with a resolution of 0.75 degrees (Dee et al. 2011) or the 55-year Japanese Reanalysis (JRA-55) with a resolution of 1.25 degrees (Kobayashi et al. 2015) are imposed to the model as the initial and boundary conditions at 6-hour interval. The National Centers for Environmental Prediction (NCEP) Real Time Global (RTG) sea surface temperature (SST) with a resolution of 0.5 degrees (http://polar.ncep.noaa.gov/sst/) was used to provide the SST to the model when driven by ERA-Interim data. The brightness temperature in two-dimensional instantaneous diagnostic fields (1.25 degrees) is used as SST for JRA-55 (Kobayashi et al. 2015). Results of the typhoon track, intensity, and wind speed are compared with the RSMC best track datasets, and the precipitation amounts in the target region validated against Automated Meteorological Data Acquisition System (AMeDAS) station observations, and Radar-AMeDAS analyzed precipitation

datasets. The warming increment data for SST, three-dimensional geopotential surface, and three-dimensional air temperature are obtained from the monthly averages of 25-year mean difference between the present-day simulation (1979–2003) and the future projection (2075–2099). The climate data are obtained from the 20 km-resolution MRI-AGCM3.2 climate simulations with the RCP-8.5 scenario (Mizuta et al. 2012, 2014).

2.3 Numerical experiments

We first conducted two numerical experiments, one experiment with JRA-55 and another experiment with ERA-Interim, to check that the suitability of the reanalysis data in representing the typhoon features. It is worth mentioning that maintaining typhoon tracks both in the actual and a future climate condition is necessary for assessing future impacts of a typhoon over a specific region (Takemi et al. 2016a, b; Mori and Takemi 2016). Thus, we have conducted a number of sensitivity experiments on the domain, physics, and nudging to capture the actual track of the typhoon (not shown here). Finally, we conducted another numerical simulation with WRF under PGW conditions, called PGW experiment. The PGW experiment method was first introduced by Sato et al. (2007) who demonstrated a simulation approach by adding global warming increments to the reanalysis. In our study, we added the warming increment data of SST, geopotential, and temperature to the JRA-55, which is found to be better compared to ERA-Interim (discussed in the results section) to perform the PGW experiment. The selection of warming increment fields is based on the previous studies of Ito et al. (2016); Takemi et al. (2016a, b); Kanada et al. (2017a). In all the three simulations, the model was initialized at 00 UTC of 26 August, 2016 and integrated till 00 UTC of 31 August, 2016.

3. The typhoon features in the present climate

We first compared the track and intensity of the typhoons represented in the reanalysis data with the RSMC best track datasets. The typhoon tracks are obtained through the minimum sea level pressure at 6-hours interval. The typhoon tracks in both the reanalysis dataset (JRA-55 and ERA-Interim) overall agree well with the best track, but the landfall locations differ by 1–2° in latitude (Fig. 2a). The central pressure of the typhoon in the reanalysis data was found to be weaker by ~40 hPa at the time of the maximum intensity and continued to be weaker until the typhoon made landfall (Fig. 3a). The maximum

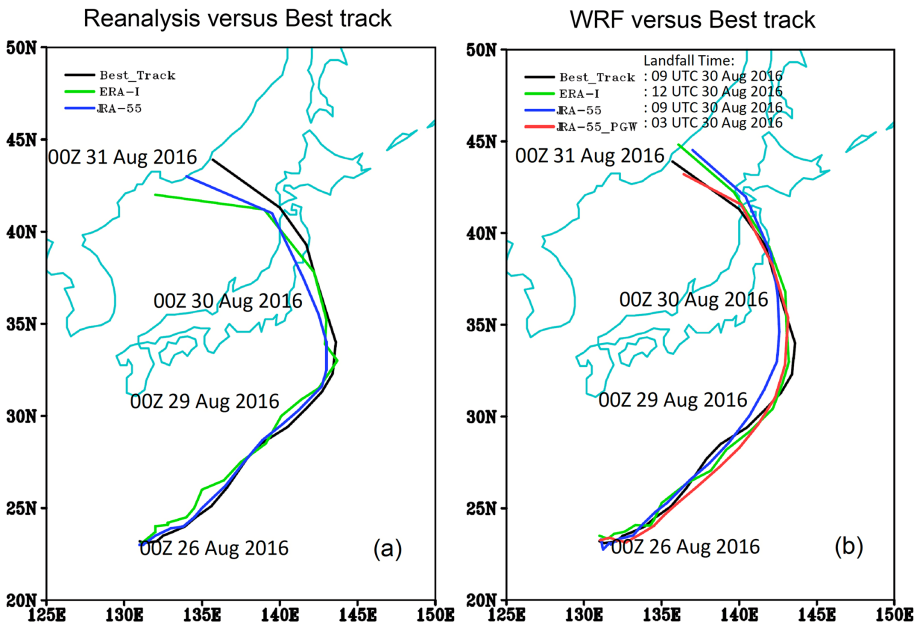

Fig. 2. Typhoon track from (a) reanalysis dataset; and (b) model simulations; and RSMC Tokyo best track data. Black color shows the tracks for RSMC, green for ERA-Interim, blue for JRA-55, and red for JRA-55 under PGW.

wind speed was also found to be weaker by about ~ 40 knots (Fig. 3c). However, the downscaled simulations with the WRF model reproduced a significant improvement in the track and intensity of the typhoon with respect to the original reanalysis datasets.

3.1 *Track and intensity*

The typhoon track in the WRF simulation with either JRA-55 or ERA-Interim being given is consistent with the RSMC best track data, especially at the landfall region (Fig. 2b). The landfall timing in the model simulation with JRA-55 closely matched with the RMSC best track, while that with ERA-Interim is delayed by 3 hours. The wind speed and central pressure are well captured by the WRF model with JRA-55 with some variations (Figs. 3b, d). In both the simulations, the typhoon made landfall over Okirai Bay area in Iwate Prefecture of Japan with the central pressure in between 950−970 hPa and the wind speed of 60−75 knots. These agree well with the RSMC

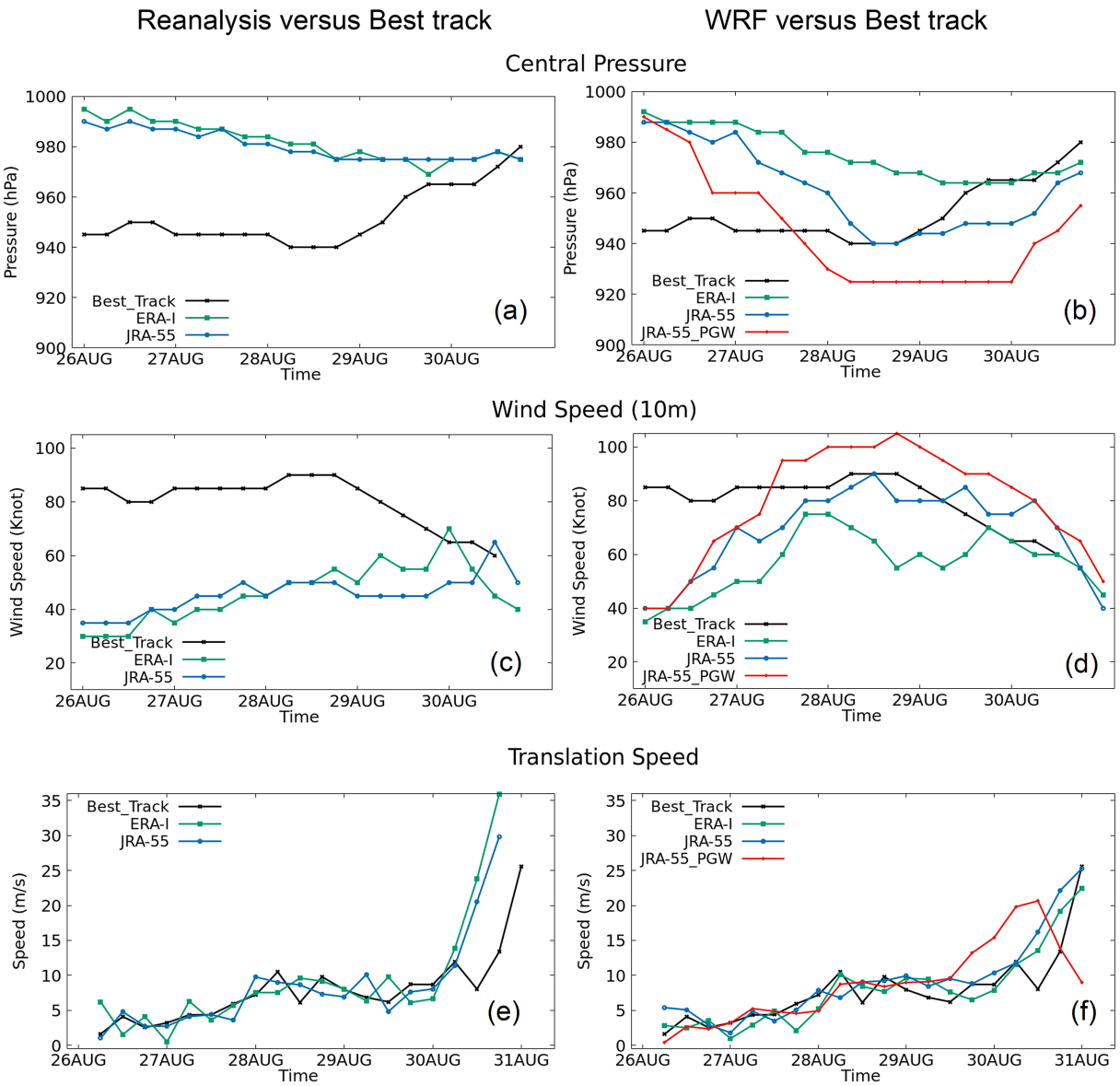

Fig. 3. Same a Fig. 2, but with central pressure (a−b); wind speed (c−d); translation speed (e−f). Translation speeds are computed from ± 6 hours typhoon location.

Tokyo best track (which showed 965 hPa central pressure and 65 knots wind speed around the same bay area). The maximum wind speed and minimum central pressure of this typhoon were found to be 90 knots and 940 hPa, respectively, in the model simulation with JRA-55, which indicates favorable results compared with RSMC. However, the simulation with JRA-55 showed stronger winds and lower central pressures even after the landfall of the typhoon. On the other hand, the simulation with ERA-Interim showed the maximum wind of 70 knots and the minimum central pressure of 960 hPa. After making landfall, the tracks in both simulations diverted slightly northward and hit the southern part of Hokkaido. The translation speed of the typhoon was computed from each simulation at a 6-hour interval from ± 6 hours typhoon location and shown in Figs. 3e and 3f. It shows that the translation speed of the typhoon in the simulation with ERA-Interim was slower compared to that of JRA-55 especially from the day before landfall. This could be a reason for the delayed landfall of the typhoon in the simulation with ERA-Interim.

The wind fields at the 850 hPa level during the passage of the typhoon over the Tohoku region are shown in Fig. 4. The simulation with JRA-55 reproduced stronger winds of more than 90 knots over wider areas during the passage of the typhoon, while the simulation with ERA-Interim shows stronger winds of more than 90 knots over comparatively smaller areas. This feature is consistent with the comparison of the surface wind speeds (Fig. 3d); the wind speed in the simulation with ERA-Interim is overall weaker than that in the others. The reduced winds represented in the simulation negatively affect the assessment of hazards at local scales.

3.2 Rainfall

Figure 5 shows the spatial distribution of precipitation amounts during the passage of the simulated typhoons over the Tohoku region. The rainfall amounts over the landfall region and its surroundings are well represented in both the simulations at the time of landfall and after landfall. The precipitation amount over the landfall region is slightly underestimated in the simulation with JRA-55, while the same is slightly overestimated in the simulation with ERA-Interim. The results indicate that the landfall region (Iwate Prefecture) including the surrounding areas in the Miyagi, Aomori, and Hokkaido prefectures experienced a heavy precipitation of greater than 50 mm h^{-1}. These results are consistent with the Radar-AMeDAS observation datasets.

The 12-hours and 24-hours accumulated precipitation amounts in the model simulations with JRA-55 as well as ERA-Interim during the landfall show a good agreement with the observation (Fig. 6). The 12-hours (24-hours) accumulated precipitation amount refers to the sum of ± 6 hours (± 12 hours) precipitation amount from the landfall time i.e., when the typhoon was active over the region. The model captured the 24-hours accumulated precipitation amounts of greater than 100 mm over the landfall region (Iwate Prefecture) and also over the surrounding regions with a maximum amount of 300 mm over central Hokkaido, which follows the observed amount over those regions. The model underestimated the precipitation amount over some regions of the domain (e.g., Aomori) and overestimated over some areas (e.g., the Okirai Bay area). The reason could be due to the deviation of the typhoon track before and after landfall. The observation shows a moderate precipitation amount over the Miyagi and Yamagata prefectures during the passage of typhoon, which is well captured by the model with JRA-55, although overestimated in some areas. On the other hand, the simulations with ERA-Interim significantly underestimate the rainfall over the Fukushima and Yamagata prefectures. Overall, the accumulated precipitation amount over the land regions shown in the figure is well captured in the model simulation with JRA-55 especially over the Tohoku region.

We next compared the simulated precipitation amounts at the grid points corresponding to 302 AMeDAS observation stations (Fig. 7). The observed results indicate that the Iwate, Aomori, and Miyagi prefectures received heavy rainfall amount (area averaged value > 50 mm) on the day of landfall. Yamagata, southern Hokkaido, and Fukushima also received ~ 35 mm precipitation during the passage of the typhoon. Both the simulations also show similar results, but with some variations (Fig. 8). The simulation with JRA-55 captured favorably averaged hourly rainfall amounts over Aomori, the southern areas of Hokkaido, Iwate, Yamagata, and Miyagi, while the simulations with ERA-Interim reproduced averaged hourly rainfall over few prefectures with nearly 3 hours delay (Fig. 9). Similar to averaged hourly precipitations, the maximum hourly precipitation was also well represented by the model with JRA-55 compared to that with ERA-Interim (Fig. 10). The maximum hourly precipitation refers to the maximum rainfall amount at a particular hour over a region. All the above results indicate that the typhoon features are captured better in the simulation driven by JRA-55

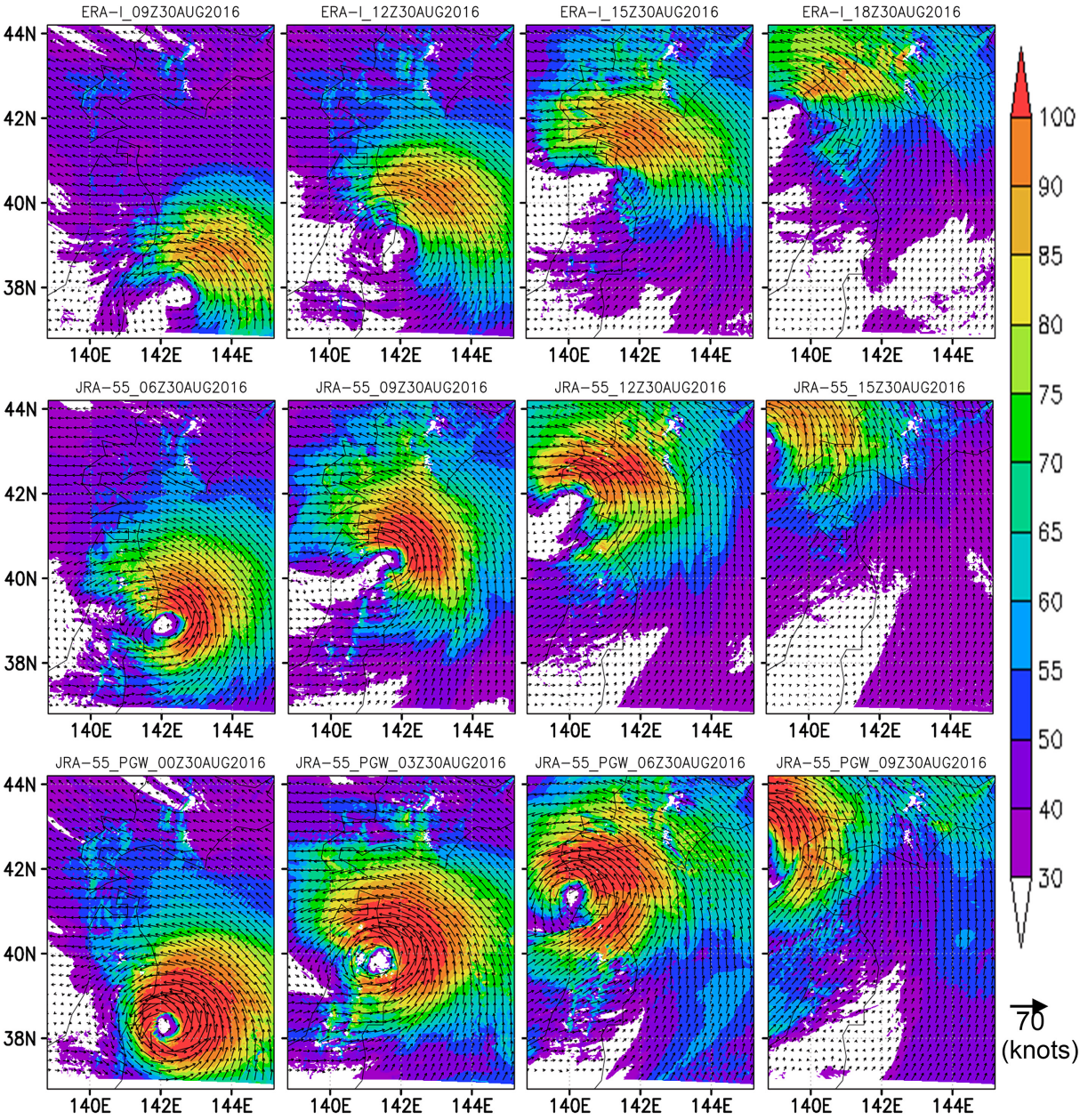

Fig. 4. Wind fields at the 850 hPa level during the passage of typhoon from the model simulation with ERA-Interim (1st row); model simulation with JRA-55 (middle row); and model simulation with JRA-55 under PGW (third row). The wind speed is indicated in knots.

than that by ERA-Interim.

Based on the results of the WRF simulations downscaled from JRA-55 and ERA-Interim, we decided to conduct PGW experiments with WRF downscaled from JRA-55. Next, we analyzed the PGW experiments with WRF driven by JRA-55 after adding the warming increment data to the reanalysis fields.

4. Impact of Typhoon Lionrock under PGW condition

The track, central pressure, wind speed, and the translation speed of the typhoon in the present climate

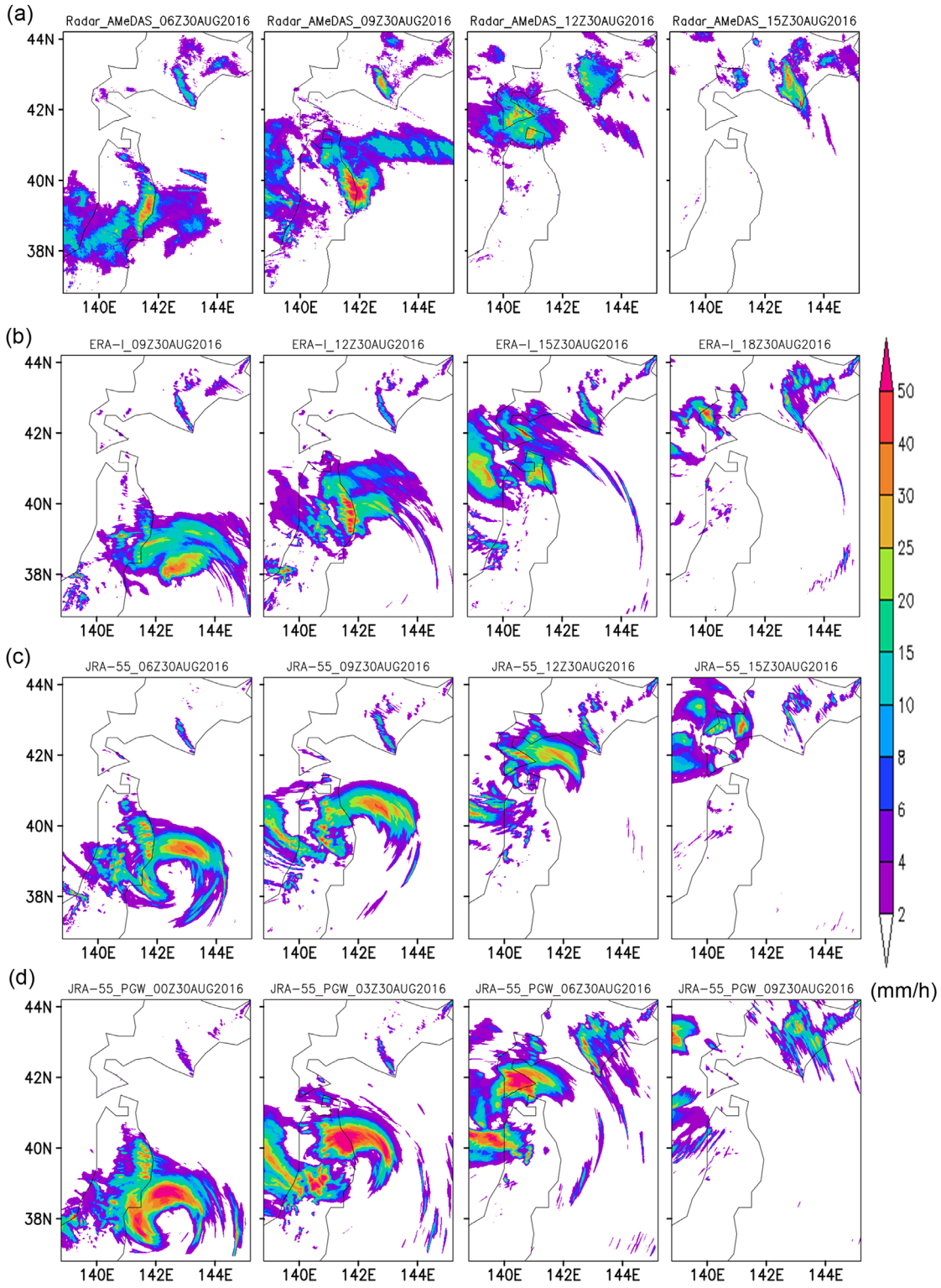

Fig. 5. Precipitation distribution during the passage of the Typhoon Lionrock from (a) Radar-AMeDAS; (b)WRF simulation with ERA-Interim; (c) WRF simulation with JRA-55; (d) WRF simulation with JRA-55 under PGW. Dates and times of the precipitation are indicated over each figure.

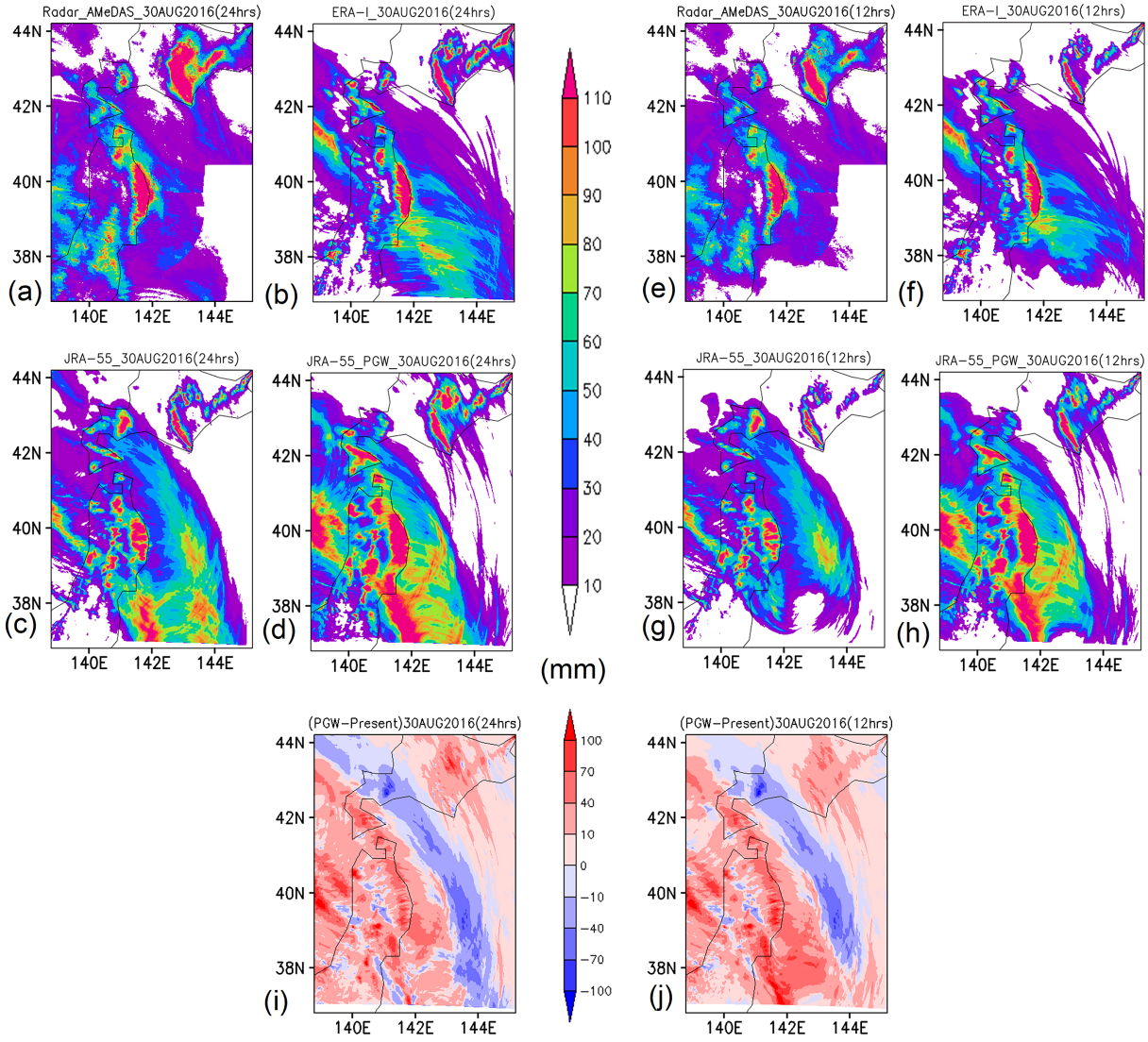

Fig. 6. 24-hours and 12-hours accumulated precipitation from (a, e) Radar-AMeDAS; (b, f) model simulation with ERA-Interim; (c, g) model simulation with JRA-55; and (d, h) model simulation with JRA-55 under PGW. Bottom two figures (i, j) shows the future change under PGW (PGW-Present) in 24hours and 12hours. The 12-hours (24-hours) accumulated rainfall corresponds to the sum of ± 6 hours (± 12 hours) precipitation amount from the landfall time of typhoon.

and the future climate are shown in Figs. 2b, 3b, 3d, and 3f respectively. It is shown that under PGW, the track remained unchanged, while the wind speed became stronger, the central pressure became lower, and the translation speed became faster, indicating the severity of the typhoon under the PGW condition. The typhoon track under PGW hit Japan at the same point as it was seen in present climate.

4.1 Intensity

The central pressure of Typhoon Lionrock is projected to become stronger up to 920 hPa in the warming climate, while it is 940 hPa in the present climate (Fig. 3b). The central pressure under PGW at the initial simulated time of 00UTC 26 August 2016 is 992 hPa, which is close to that in present climate (which is 995 hPa). However, the central pressure of the typhoon under PGW becomes stronger after 12

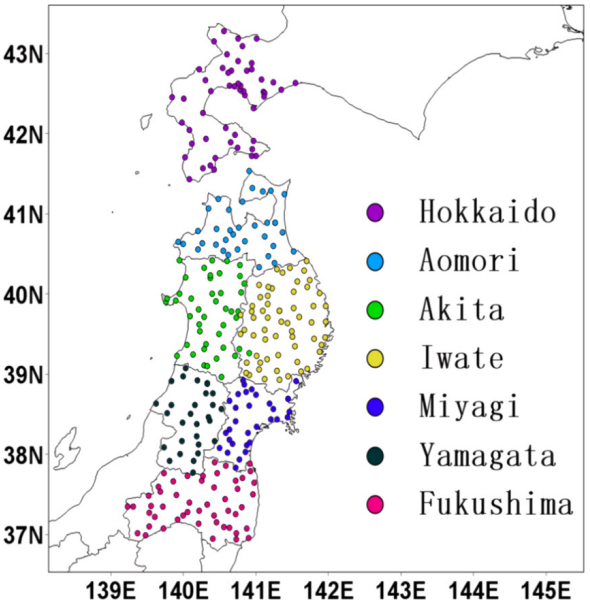

Fig. 7. Location of the 302 AMeDAS observation stations at which the precipitations are analyzed quantitatively during the passage of typhoon

hours and reaches at ~ 920 hPa at 06UTC 28 August 2016 and continues until it makes landfall (until 00 UTC 30 August 2016). Figure 3d represents the wind at the 10 m height in the present climate and under PGW conditions. It is clearly shown that the wind speed of the typhoon is increased by ~ 10 knots at the time of landfall under PGW conditions. The translation speed of the typhoon under PGW is also increased by about 10 m s^{-1} from the day before its landfall. The spatial distribution of the wind at 850 hPa during the landfall under PGW is shown in Fig. 4. It also indicates that the wind speed is increased not only at the landfall region but also over the surrounding prefectures as well as over the ocean basins. The two days (29–30 August) mean wind speed at 850 hPa also shows an increase of wind speed over northern Japan (Fig. 11). The increased winds may cause storm surge damage (e.g., Farfan et al. 2014) to the coastal Tohoku region under future climate. The increase of wind speed under future climates was also identified in the previous studies (e.g., Mei and Xie 2016; Takemi et al. 2016b), which highlighted the future increase of wind speed for other typhoons. We find that Typhoon Lionrock under PGW will approach faster by about 6 hours and pass the Tohoku region more quickly, probably

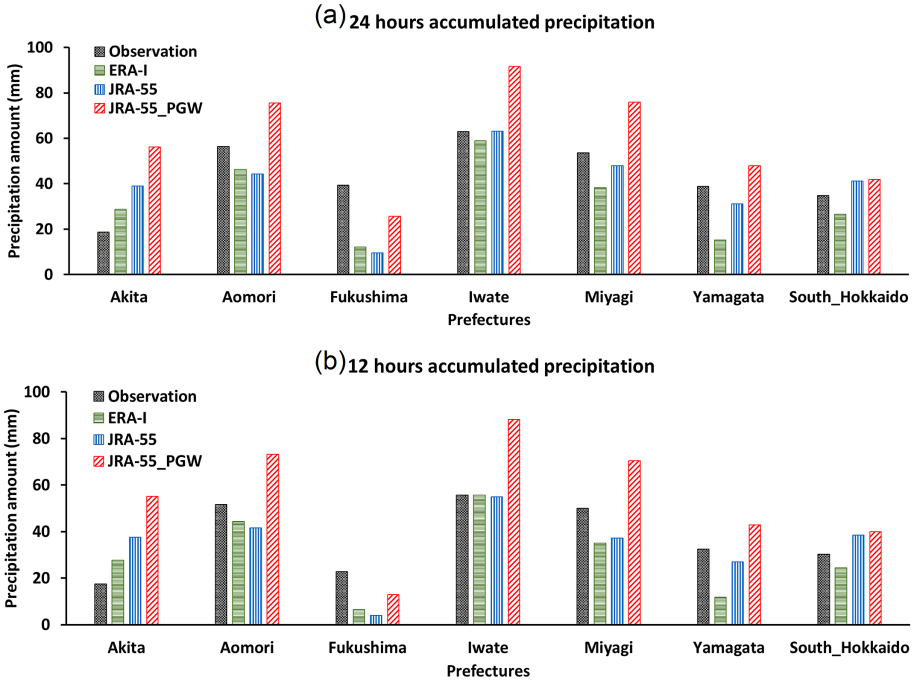

Fig. 8. 24-hours (a) and 12-hours (b) accumulated rainfall over each prefecture during the passage of the typhoon as described in Fig. 6.

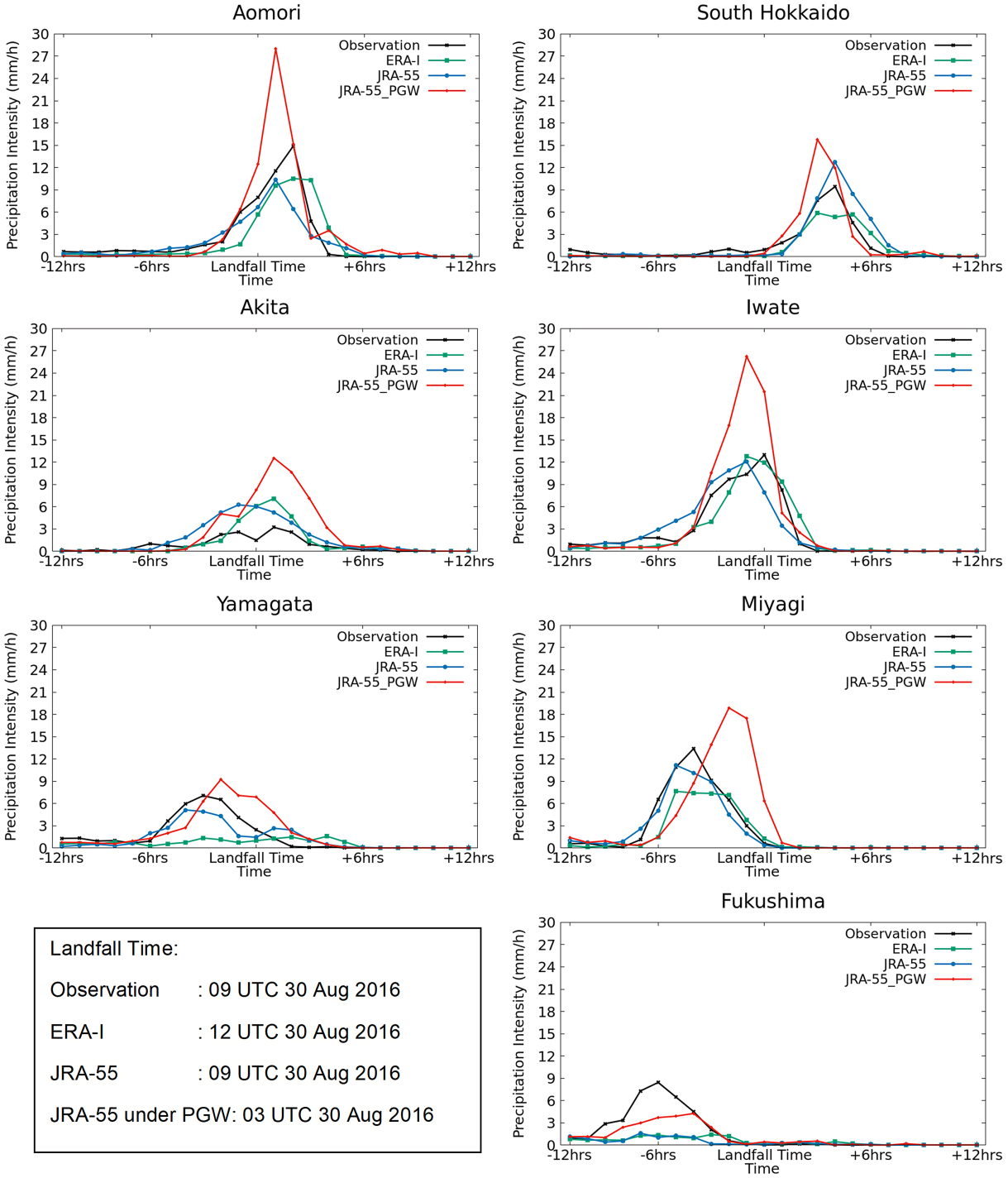

Fig. 9. Averaged hourly precipitation on the day of landfall over each prefecture from AMeDAS station observations (black);(b) model simulation with ERA-Interim (green); model simulation with JRA-55 (blue); and model simulation with JRA-55 under PGW (red).

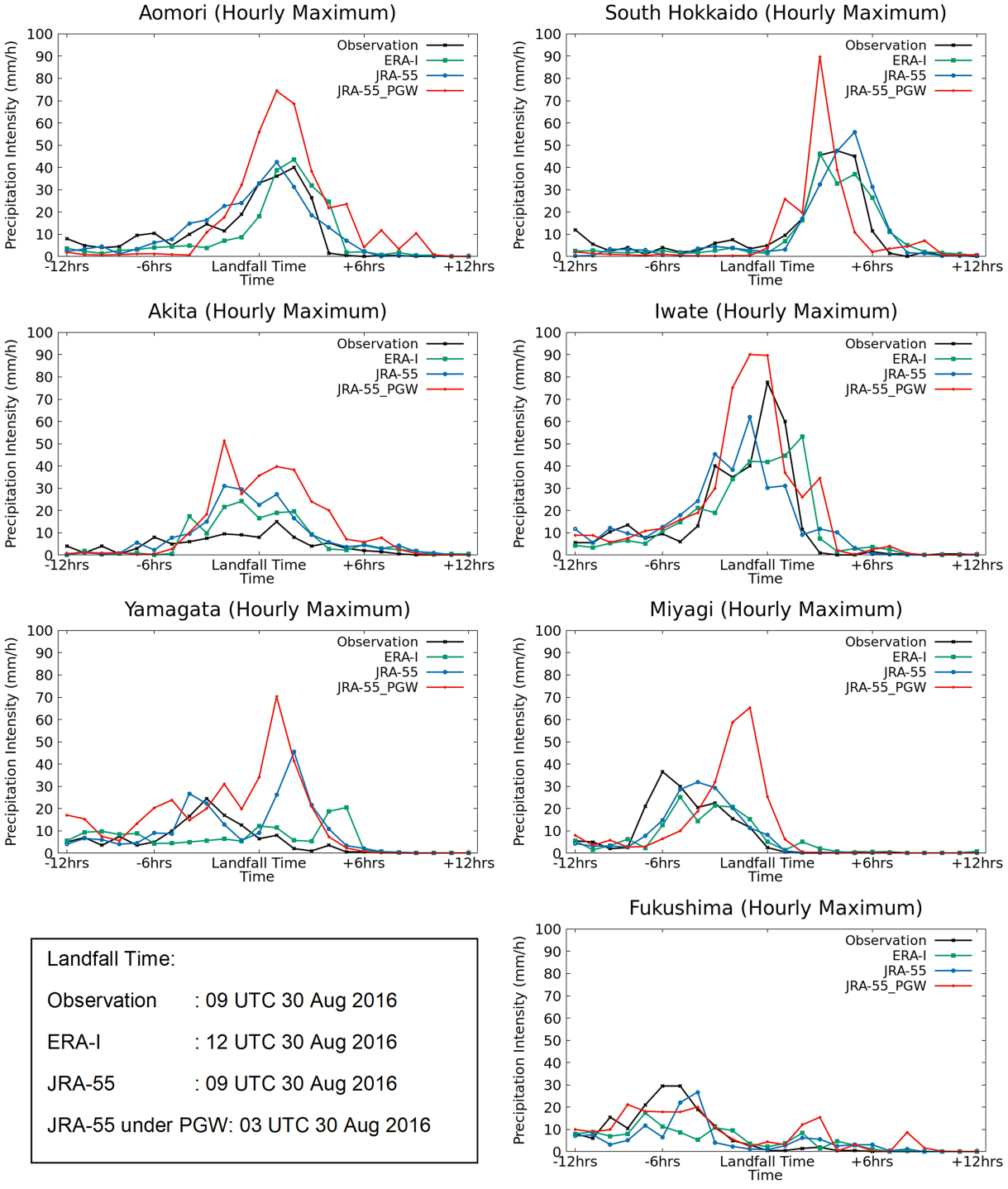

Fig. 10. Same as Fig. 9, but for maximum hourly precipitation. It corresponds to the maximum rainfall amount at a particular hour over a region.

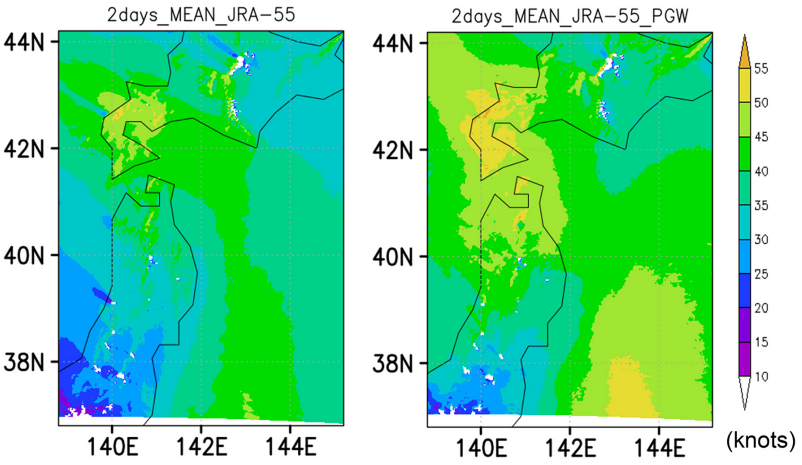

Fig. 11. Two days (29–30 August) mean wind at 850 hPa in present climate and under PGW.

due to faster translation speed of the typhoon under PGW conditions (Fig. 3f). Our findings of increased wind speed are different from previous studies (e.g., Takemi et al. 2016a; Ito et al. 2016), which showed that the wind speeds of Typhoon Mireille (1991) and Typhoon Songda (2004) weakened over the northern part of Japan under PGW conditions. We speculate the reason could be associated with the approaching direction of the typhoon and the location. Typhoon Mireille (1991) and Typhoon Songda (2004) approached from the southwest over the Sea of Japan, while Typhoon Lionrock (2016) approached from the southeast over the Pacific Ocean.

4.2 Rainfall

The future changes in the precipitation during the landfall of the typhoon are shown in Figs. 6 and 8. The precipitation amounts associated with Typhoon Lionrock are found to be increased under PGW conditions over all prefectures. The 24-hours and 12-hours accumulated rainfalls are also found to be increased by ~70 mm over some areas of Hokkaido, Iwate, Aomori, Miyagi and Akita regions (Fig. 6). The increase of precipitation over Hokkaido region in warming climate is also highlighted in Kanada et al. (2017a) due to passage of Typhoon Chanthu (2016). We quantified the 24-hours and 12-hours total precipitation amounts averaged over each prefecture under PGW condition at 302 AMeDAS stations, which are shown in Fig. 8. We find that the precipitation amount associated with the typhoon is increased over entire Tohoku region in future climate. Iwate, Aomori, Akita, and Miyagi are projected to experience more precipitation ($>$ 20 mm) under PGW condition, indicating an increased risk of flooding over these regions. The changes in hourly precipitations under warming climate is also noticed to be doubled over Aomori, Iwate, Akita, and Miyagi prefectures (Fig. 9) with maximum hourly precipitation amount of 50–90 mm at some station points (Fig. 10). It is worthy to mention that the total precipitation amount over the target region may be different (less or more) in future climate due to the shorter passage time of future typhoon because of its faster translation speed. But this is unclear and dependent on other factors, e.g., typhoon size of future typhoon, because larger typhoons may continue rain for a longer time as it has a large radius of a gale-force wind. However, this could be on another research and kept outside of this study.

5. Discussion and conclusions

In this study, by using the WRF model driven by two reanalysis datasets, JRA-55 and ERA-Interim, we performed dynamical downscaling simulations of a typhoon, which had an unusual track in the recorded history of JMA. Our results indicate that the WRF forced by JRA-55 reproduced the features of Typhoon Lionrock (2016) better than that forced by ERA-Interim. We found that the typhoon track was well captured by the model, especially the landfall region. The landfall time (i.e., 09 UTC 30 August 2016) was accurately captured in the simulation with JRA-55, while the landfall time was delayed by 3 hours in the case of ERA-Interim (landfall at 12 UTC 30 August 2016). The delayed landfall by the model with ERA-Interim could be associated with the translation

speed, which was determined by the steering flow during the movement of the typhoon. To understand the mechanism, we analyzed the wind steering at 500 hPa on 29 August 2016 and 30 August 2016. This is shown in Fig. 12. It clearly indicates that the typhoon in the simulation with ERA-Interim moved slowly compared to that of JRA-55. The location of the typhoon in both simulations shows nearly at (31N, 142E) in the steering wind on 29 August. However, on 30 August, the location of the typhoon in the simulation with JRA-55 was found at a higher latitude compared to that of ERA-Interim (about 2° higher in the case of JRA-55). Although initial position, central pressure and wind speed were closely the same in the both reanalysis datasets, i.e., JRA-55 and ERA-Interim, the central pressure remained higher and wind speed continued weaker until the landfall compared to the observation in the case of ERA-Interim (Figs. 3b, d). Previous studies (e.g., Islam et al. 2015; Parker et al. 2017) also documented that the WRF simulation with ERA-Interim data underestimated the strength of tropical cyclones. In the case of JRA-55, the central pressure and wind speed had a good agreement after about 2 days of simulation and then followed the best track observations. Our results also indicated that precipitation amounts over the landfall region are well represented in the model simulations and closely followed the Radar-AMeDAS observations. Overall analysis from the simulations of the actual typhoon, we find that the model with JRA-55 represent the features of Typhoon Lionrock better than the model with ERA-Interim.

We next examined the impacts of Typhoon Lionrock under future climate by conducting PGW experiments using JRA-55. We found a resembled typhoon track with stronger wind speed (by ~ 20 knots), lower central pressure (by ~ 20 hPa), and faster translation speed (by ~ 1 m s^{-1}) under PGW. Takemi et al. (2016b) also reported an increase in wind speed and decrease in central pressure for Typhoon Vera (1959) under PGW. The steering wind at 500 hPa also showed that the typhoon under PGW moved faster compared to that in present climate (Fig. 12) and made an earlier landfall by ~ 6 hours. This can be seen from the location of the typhoon in Fig. 12. The location of the typhoon shows nearly at (31N, 142E) in the steering wind on 29 August in present as well as in future climate. However, on 30 August, the location of the typhoon is found nearly at (40N, 142E) in present, which is nearly at (42N, 140E) in future climate. The reason of stronger intensity of the typhoon in warming climate could be associated with the increase in SST and atmospheric moisture content (Mousavi et al. 2009; Takemi et al. 2012; Camargo et al. 2013; Lin et al. 2014; Mei et al. 2015; Mei and Xie 2016; Parker et al. 2018). The SST and surface water vapor in present climate and those under PGW are shown in Fig. 13. It clearly indicates an increase of SST (Fig. 13a) and surface water vapor as well (Fig. 13b). Increase of SST enhances surface water vapor fluxes from the ocean surface. This considerable increase was equivalent to potential temperature (Črnivec et al. 2016) and the buoyancy in the atmosphere (Seeley and Romps 2015). As a result, the rate of radial gradient of diabatic heating increased and led to stronger overturning circulation in the low to middle troposphere above the boundary layer. As a consequence, the radial import of absolute angular momentum surfaces becomes stronger, leading to faster spin up and making stronger the typhoon intensity (Črnivec et al. 2016). We also analyzed the vertical profile of water vapor in the present and future climates and found an increase of water vapor at each pressure level under PGW, which was gradually decreased from the surface (Fig. 13c). This implies that the water vapor in the future climate is increased not only at the surface but also at an upper layer. The increased moisture at the upper layer is in general favorable for the development of sustained convection (Takemi et al. 2004; Unuma and Takemi 2016), and could feed more moisture to the typhoon and make it stronger in the future climate.

We further found that the precipitation associated with Typhoon Lionrock was increased significantly under PGW compared to that in the present climate. We found that the rainfall amount during the passage of typhoon was increased by more than 20 mm over the Akita, Aomori, Iwate, and Hokkaido prefectures. The increase of precipitation intensitied over Japan under a warming climate was reported in many studies (e.g., Nayak and Dairaku 2016; Yamada et al. 2017; Nayak et al. 2018). The reason could be due to the increase of water vapor under warmer air temperature according to the Clausius-Clapeyron relationship, which is expected to increase at a rate of ~ 7 % per each degree rise in temperature (Trenberth 2003). Increase of SST under PGW conditions could be another cause for the increase of precipitation associated with the typhoon in future climate. Lin et al. (2015) reported that a 3°C increase in SST may increase the rainfall associated by tropical cyclone by ~ 22.5 %. Our study shows about 5°C increase of SST over northern Japan in the future climate (Fig. 13a). This may lead to increase in moisture availability in the warming climate (nearly 4 g kg^{-1} increase at surface, Fig. 13b)

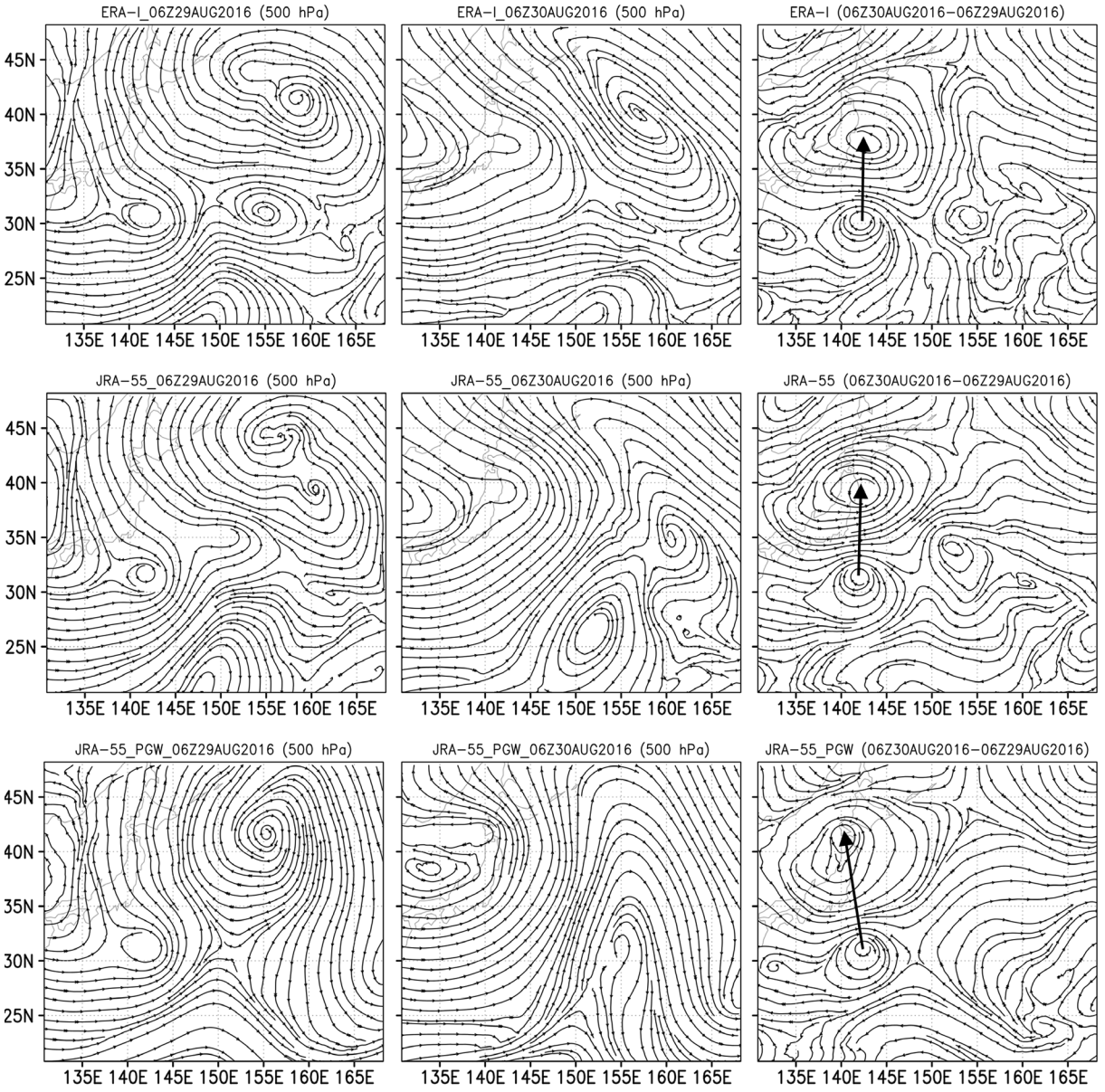

Fig. 12. Wind steering at 500 hPa on 06 UTC of 29 August 2016 (1st column); 06 UTC of 30 August 2016 (2nd column); and their differences (3rd column). 1st row corresponds the results from the simulation with ERA-Interim, 2nd and 3rd rows correspond the results from the simulations with JRA-55 and JRA-55 under PGW respectively. The arrows indicate the direction and location of the typhoon traveled during 06 UTC of 29 August to 06 UTC of 30 August.

and hence, stronger convective instability (Kanada et al. 2017a). This may lead to produce more precipitation over the Tohoku region in the future climate. To further understand the mechanism for the increase in precipitation intensity under PGW, we analyzed convective available potential energy (CAPE) on the day before the landfall (i.e., 29 August) in the present climate and the future climate. We identified that the CAPE under PGW conditions corresponded to higher values (> 2000 J Kg^{-1}) on the day before the landfall, while the same in present climate corresponded to ~ 800 J Kg^{-1} (Fig. 14). This implies that the CAPE

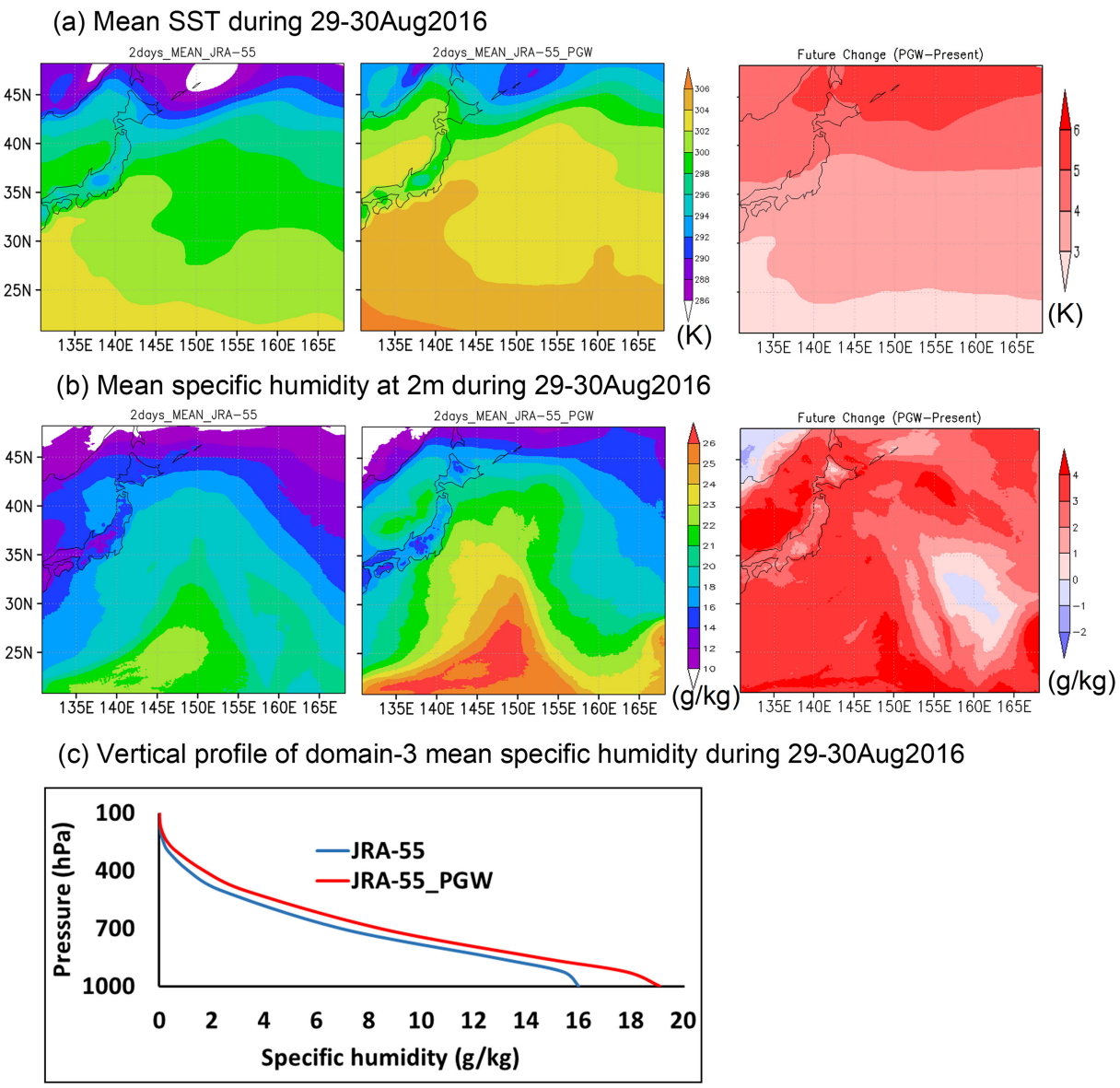

Fig. 13. (a) Two days mean SST; (b) two days mean specific humidity at 2 m; and (c) vertical profile of two days domain (domain-3) mean. The two days correspond to 29 August 2016 and 30 August 2016. Domain-3 corresponds to the innermost domain of our study (i.e., 138–146E, 37–45N).

under PGW condition is expected to be significantly higher compared to that in the present climate, indicating more amount of energy will be available for convection under PGW. This may also lead to more precipitation in the future climate. We speculate the CAPE may be increased due to the increase of specific humidity because the comparison between specific humidity and CAPE (Figs. 13, 14) showed a good correlation in increasing the water vapor and that of CAPE. Closer investigation indicates that the CAPE under PGW conditions was higher over the Aomori, Iwate, and Hokkaido prefectures. This could be a reason of increased precipitation over the northern part of the Japan in future climate (Figs. 14, 6). It is worthy to mention that the time difference between the CAPE in the present and the future climate should be the same with the difference in landfall timings of the typhoon in the present and the future climate.

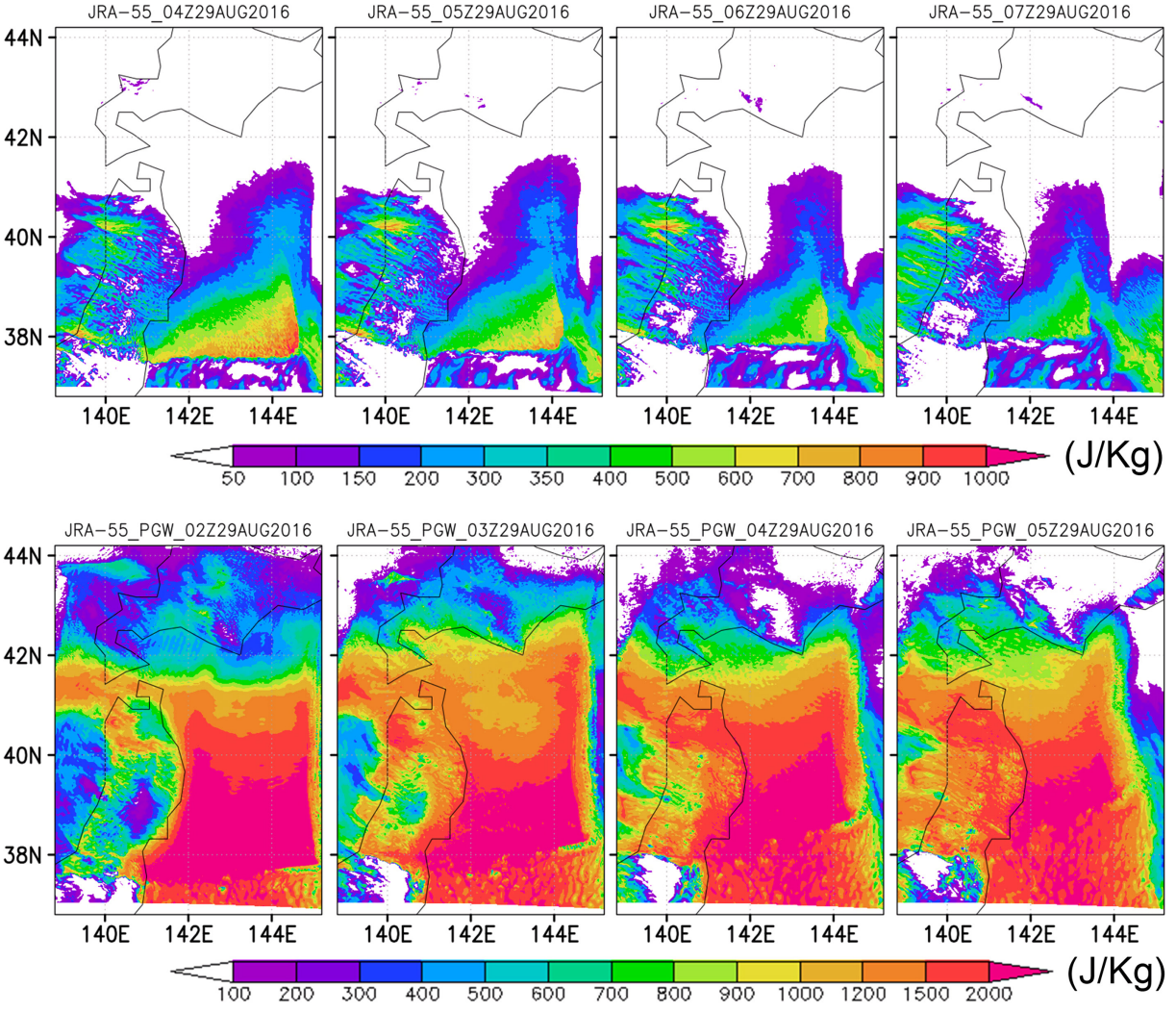

Fig. 14. CAPE on the day before of the typhoon made landfall from the model simulation with JRA-55 (top row); and JRA-55 under PGW (bottom row). Dates and times of the precipitation are indicated over each figure. The CAPE is indicated in J Kg^{-1}.

However, we find that the time difference between the CAPE in the present and the future climate is 2 hours, whereas the time difference between the landfall timing of the typhoon in the present and the future climate is noted as 6 hours. This four-hour variation between the time differences of CAPE and landfall of typhoon in two climate periods could be due to the faster movement of the typhoon in the future climate.

The present study overall demonstrated that the downscaled simulations with WRF model reproduced a significant improvement in the track and intensity of the typhoon with respect to the original reanalysis datasets and the downscaled precipitations over the landfall region in the present climate condition and agree well with the observations. The typhoon is projected to be stronger and more powerful under future warm climate. It is expected to produce more precipitation over Hokkaido and the entire Tohoku region in warming climate. The study suggests that the typhoons under PGW condition may increase the risk of flooding, damages to infrastructures, and lives along the typhoon track. However, to reveal the robust features of typhoon hazards under global warming, we would like to further analyze the other type of devastating typhoons that made landfall over northern Japan.

Acknowledgments

We would like to thank two anonymous reviewers for their useful and constructive comments in improving the original manuscript. This study is supported by the TOUGOU Program, funded by the Ministry of Education, Culture, Sports, Science, and Technology, Government of Japan. Japan Meteorological Agency (JMA) is acknowledged for providing the Automated Meteorological Data Acquisition System (AMeDAS) data. We acknowledge the Regional Specialized Meteorological Center (RSMC) Tokyo -Typhoon Center for making available the typhoon best tract dataset. The Disaster Prevention Research Institute (DPRI), Kyoto University is acknowledged for providing the research facilities.

References

Aon Benfield, 2016: *Global Catastrophe Recap – October 2016*. [Available at http://thoughtleadership.aonbenfield.com/pages/Home.aspx?ReportYear=2016.]

Camargo, S. J., M. Ting, and Y. Kushnir, 2013: Influence of local and remote SST on North Atlantic tropical cyclone potential intensity. *Climate Dyn.*, **40**, 1515–1529.

Chen, C.-J., T.-Y. Lee, C.-M. Chang, and J.-Y. Lee, 2018: Assessing typhoon damages to Taiwan in the recent decade: Return period analysis and loss prediction. *Nat. Hazards*, **91**, 759–783.

Črnivec, N., R. K. Smith, and G. Kilroy, 2016: Dependence of tropical cyclone intensification rate on sea-surface temperature. *Quart. J. Roy. Meteor. Soc.*, **142**, 1618–1627.

Dee, D. P., S. M. Uppala, A. J. Simmons, P. Berrisford, P. Poli, S. Kobayashi, U. Andrae, M. A. Balmaseda, G. Balsamo, P. Bauer, P. Bechtold, A. C. M. Beljaars, L. van de Berg, J. Bidlot, N. Bormann, C. Delsol, R. Dragani, M. Fuentes, A. J. Geer, L. Haimberger, S. B. Healy, H. Hersbach, E. V. Hólm, L. Isaksen, P. Kållberg, M. Köhler, M. Matricardi, A. P. McNally, B. M. Monge-Sanz, J.-J. Morcrette, B. K. Park, C. Peubey, P. de Rosnay, C. Tavolato, J.-N. Thépaut, and F. Vitart, 2011: The ERA-Interim reanalysis: Configuration and performance of the data assimilation system. *Quart. J. Roy. Meteor. Soc.*, **137**, 553–597.

Emanuel, K., 2005: Increasing destructiveness of tropical cyclones over the past 30 years. *Nature*, **436**, 686–688.

Farfán, L. M., E. J. D'Sa, K. Liu, and V. H. Rivera-Monroy, 2014: Tropical cyclone impacts on coastal regions: The case of the Yucatán and the Baja California Peninsulas, Mexico. *Estuaries Coasts*, **37**, 1388–1402.

Guan, S., S. Li, Y. Hou, P. Hu, Z. Liu, and J. Feng, 2018: Increasing threat of landfalling typhoons in the western North Pacific between 1974 and 2013. *Int. J. Appl. Earth Observ. Geoinform.*, **68**, 279–286.

Hong, S.-Y., and J.-O. J. Lim, 2006: The WRF single-moment 6-class microphysics scheme (WSM6). *J. Korean Meteor. Soc.*, **42**, 129–151.

Hong, S.-Y., Y. Noh, and J. Dudhia, 2006: A new vertical diffusion package with an explicit treatment of entrainment processes. *Mon. Wea. Rev.*, **134**, 2318–2341.

IPCC, 2013: *Climate Change 2013: The Physical Science Basis. Contribution of Working Group I to the Fifth Assessment Report of the Intergovernmental Panel on Climate Change*. Stocker, T. F., D. Qin, G.-K. Plattner, M. M. B. Tignor, S. K. Allen, J. Boschung, A. Nauels, Y. Xia, V. Bex, and P. M. Midgley (eds.), Cambridge University Press, Cambridge, UK and New York, USA, 1535 pp.

IPCC, 2014: *Climate Change 2014: Impacts, Adaptation, and Vulnerability. Part A: Global and Sectoral Aspects. Contribution of Working Group II to the Fifth Assessment Report of the Intergovernmental Panel on Climate Change*. Field, C. B., V. R. Barros, D. J. Dokken, K. J. Mach, M. D. Mastrandrea, T. E. Bilir, M. Chatterjee, K. L. Ebi, Y. O. Estrada, R. C. Genova, B. Girma, E. S. Kissel, A. N. Levy, S. MacCracken, P. R. Mastrandrea, and L. L. White (eds.), Cambridge University Press, Cambridge, UK and New York, USA, 1132 pp.

Islam, T., P. K. Srivastava, M. A. Rico-Ramirez, Q. Dai, M. Gupta, and S. K. Singh, 2015: Tracking a tropical cyclone through WRF–ARW simulation and sensitivity of model physics. *Nat. Hazards*, **76**, 1473–1495.

Ito, R., T. Takemi, and O. Arakawa, 2016: A possible reduction in the severity of typhoon wind in the northern part of Japan under global warming: A case study. *SOLA*, **12**, 100–105.

Kain, J. S., and J. M. Fritsch, 1993: Convective parameterization for mesoscale models: The Kain–Fritsch scheme. *The Representation of Cumulus Convection in Numerical Models*. Meteor. Monogr., No. 46, Amer. Meteor. Soc., 165–170.

Kanada, S., K. Tsuboki, H. Aiki, S. Tsujino, and I. Takayabu, 2017a: Future enhancement of heavy rainfall events associated with a typhoon in the midlatitude regions. *SOLA*, **13**, 246–251.

Kanada, S., T. Takemi, M. Kato, S. Yamasaki, H. Fudeyasu, K. Tsuboki, O. Arakawa, and I. Takayabu, 2017b: A multimodel intercomparison of an intense typhoon in future, warmer climates by four 5-km-mesh models. *J. Climate*, **30**, 6017–6036.

Knutson, T. R., J. L. McBride, J. Chan, K. Emanuel, G. Holland, C. Landsea, I. Held, J. P. Kossin, A. K. Srivastava, and M. Sugi, 2010: Tropical cyclones and climate change. *Nat. Geosci.*, **3**, 157–163.

Kobayashi, S., Y. Ota, Y. Harada, A. Ebita, M. Moriya, H. Onoda, K. Onogi, H. Kamahori, C. Kobashi, H. Endo, K. Miyaoka, and K. Takahashi, 2015: The JRA-55

Reanalysis: General specifications and basic characteristics. *J. Meteor. Soc. Japan*, **93**, 5–48.

Kure, S., Y. Jibiki, M. Quimpo, U. N. Manalo, Y. Ono, and A. Mano, 2016: Evaluation of the characteristics of human loss and building damage and reasons for the magnification of damage due to Typhoon Haiyan. *Coastal Eng. J.*, **58**, 1640008, doi:10.1142/S0578563416400088.

Lavender, S. L., and K. J. E. Walsh, 2011: Dynamically downscaled simulations of Australian region tropical cyclones in current and future climates. *Geophys. Res. Lett.*, **38**, L10705, doi:10.1029/2011GL047499.

Lin, I.-I., I.-F. Pun, and C.-C. Lien, 2014: "Category-6" supertyphoon Haiyan in global warming hiatus: Contribution from subsurface ocean warming. *Geophys. Res. Lett.*, **41**, 8547–8553.

Lin, Y., M. Zhao, and M. Zhang, 2015: Tropical cyclone rainfall area controlled by relative sea surface temperature. *Nat. Commun.*, **6**, 6591, doi:10.1038/ncomms7591.

Mei, W., and S.-P. Xie, 2016: Intensification of landfalling typhoons over the northwest Pacific since the late 1970s. *Nat. Geosci.*, **9**, 753–757.

Mei, W., S.-P. Xie, F. Primeau, J. C. McWilliams, and C. Pasquero, 2015: Northwestern Pacific typhoon intensity controlled by changes in ocean temperatures. *Sci. Adv.*, **1**, e1500014, doi:10.1126/sciadv.1500014.

Mendelsohn, R., K. Emanuel, S. Chonabayashi, and L. Bakkensen, 2012: The impact of climate change on global tropical cyclone damage. *Nat. Climate Change*, **2**, 205–209.

Mizuta, R., H. Yoshimura, H. Murakami, M. Matsueda, H. Endo, T. Ose, K. Kamiguchi, M. Hosaka, M. Sugi, S. Yukimoto, S. Kusunoki, and A. Kitoh, 2012: Climate simulations using MRI-AGCM3.2 with 20-km grid. *J. Meteor. Soc. Japan*, **90A**, 233–258.

Mizuta, R., O. Arakawa, T. Ose, S. Kusunoki, H. Endo, and A. Kitoh, 2014: Classification of CMIP5 future climate responses by the tropical sea surface temperature changes. *SOLA*, **10**, 167–171.

Mlawer, E. J., S. J. Taubman, P. D. Brown, M. J. Iacono, and S. A. Clough, 1997: Radiative transfer for inhomogeneous atmospheres: RRTM, a validated correlated-k model for the longwave. *J. Geophys. Res.*, **102**, 16663–16682.

Mori, N., and T. Takemi, 2016: Impact assessment of coastal hazards due to future changes of tropical cyclones in the North Pacific Ocean. *Weather Climate Extremes*, **11**, 53–69.

Mori, N., M. Kato, S. Kim, H. Mase, Y. Shibutani, T. Takemi, K. Tsuboki, and T. Yasuda, 2014: Local amplification of storm surge by Super Typhoon Haiyan in Leyte Gulf. *Geophys. Res. Lett.*, **41**, 5106–5113.

Mousavi, M. E., J. L. Irish, A. E. Frey, F. Olivera, and B. L. Edge, 2009: Global warming and hurricanes: The potential impact of hurricane intensification and sea level rise on coastal flooding. *Climate Change*, **104**, 575–597.

Murakami, H., Y. Wang, H. Yoshimura, R. Mizuta, M. Sugi, E. Shindo, Y. Adachi, S. Yokimoto, M. Hosaka, S. Kusunoki, T. Ose, and A. Kitoh, 2012: Future changes in tropical cyclone activity projected by the new high-resolution MRI-AGCM. *J. Climate*, **25**, 3237–3260.

Nakamura, R., T. Shibayama, M. Esteban, and T. Iwamoto, 2016: Future typhoon and storm surges under different global warming scenarios: Case study of typhoon Haiyan (2013). *Nat. Hazards*, **82**, 1645–1681.

Nayak, S., and K. Dairaku, 2016: Future changes in extreme precipitation intensities associated with temperature under SRES A1B scenario. *Hydrol. Res. Lett.*, **10**, 139–144.

Nayak, S., K. Dairaku, I. Takayabu, A. Suzuki-Parker, and N. N. Ishizaki, 2018: Extreme precipitation linked to temperature over Japan: Current evaluation and projected changes with multi-model ensemble downscaling. *Climate Dyn.*, **51**, 4385–4401.

Nishijima, K., T. Maruyama, and M. Graf, 2012: A preliminary impact assessment of typhoon wind risk of residential buildings in Japan under future climate change. *Hydrol. Res. Lett.*, **6**, 23–28.

Oku, Y., T. Takemi, H. Ishikawa, S. Kanada, and M. Nakano, 2010: Representation of extreme weather during a typhoon landfall in regional meteorological simulations: A model intercomparison study for Typhoon Songda (2004). *Hydrol. Res. Lett.*, **4**, 1–5.

Parker, C. L., A. H. Lynch, and P. A. Mooney, 2017: Factors affecting the simulated trajectory and intensification of Tropical Cyclone Yasi (2011). *Atmos. Res.*, **194**, 27–42.

Parker, C. L., C. L. Bruyère, P. A. Mooney, and A. H. Lynch, 2018: The response of land-falling tropical cyclone characteristics to projected climate change in northeast Australia. *Climate Dyn.*, **51**, 3467–3485.

Sato, T., F. Kimura, and A. Kitoh, 2007: Projection of global warming onto regional precipitation over Mongolia using a regional climate model. *J. Hydrol.*, **333**, 144–154.

Seeley, J. T., and D. M. Romps, 2015: Why does tropical convective available potential energy (CAPE) increase with warming? *Geophys. Res. Lett.*, **42**, 10429–10437.

Skamarock, W. C., J. B. Klemp, J. Dudhia, D. O. Gill, D. M. Barker, M. G. Duda, X. Huang, W. Wang, and J. G. Powers, 2008: *A description of the advanced research WRF version 3*. NCAR Tech. Note, NCAR/TN-475+STR, National Center For Atmospheric Research, Boulder, Co, USA, Mesoscale and Microscale Meteorology Division, 113 pp.

Staid, A., S. D. Guikema, R. Nateghi, S. M. Quiring, and M. Z. Gao, 2014: Simulation of tropical cyclone impacts to the US power system under climate change scenarios. *Climate Change*, **127**, 535–546.

Sugi, M., A. Noda, and N. Sato, 2002: Influence of the global warming on tropical cyclone climatology: An experiment with the JMA global model. *J. Meteor. Soc. Japan*, **80**, 249–272.

Takayabu, I., K. Hibino, H. Sasaki, H. Shiogama, N. Mori, Y. Shibutani, and T. Takemi, 2015: Climate change effects on the worst-case storm surge: A case study of Typhoon Haiyan. *Environ. Res. Lett.*, **10**, 064011, doi: 10.1088/1748-9326/10/6/064011.

Takemi, T., O. Hirayama, and C. Liu, 2004: Factors responsible for the vertical development of tropical oceanic cumulus convection. *Geophys. Res. Lett.*, **31**, L11109, doi:10.1029/2004GL020225.

Takemi, T., S. Nomura, Y. Oku, and H. Ishikawa, 2012: A regional-scale evaluation of changes in environmental stability for summertime afternoon precipitation under global warming from super-high-resolution GCM simulations: A study for the case in the Kanto Plain. *J. Meteor. Soc. Japan*, **90A**, 189–212.

Takemi, T., R. Ito, and O. Arakawa, 2016a: Effects of global warming on the impacts of Typhoon Mireille (1991) in the Kyushu and Tohoku regions. *Hydrol. Res. Lett.*, **10**, 81–87.

Takemi, T., R. Ito, and O. Arakawa, 2016b: Robustness and uncertainty of projected changes in the impacts of Typhoon Vera (1959) under global warming. *Hydrol. Res. Lett.*, **10**, 88–94.

Takemi, T., Y. Okada, R. Ito, H. Ishikawa, and E. Nakakita, 2016c: Assessing the impacts of global warming on meteorological hazards and risks in Japan: Philosophy and achievements of the SOUSEI program. *Hydrol. Res. Lett.*, **10**, 119–125.

Trenberth, K. E., A. Dai, R. M. Rasmussen, and D. B. Parsons, 2003: The changing character of precipitation. *Bull. Amer. Meteor. Soc.*, **84**, 1205–1217.

Unuma, T., and T. Takemi, 2016: Characteristics and environmental conditions of quasi-stationary convective clusters during the warm season in Japan. *Quart. J. Roy. Meteor. Soc.*, **142**, 1232–1249.

Yamada, Y., M. Satoh, M. Sugi, C. Kodama, A. T. Noda, M. Nakano, and T. Nasuno, 2017: Response of tropical cyclone activity and structure to global warming in a high-resolution global nonhydrostatic model. *J. Climate*, **30**, 9703–9724.